JOURNAL OF GEOPHYSICAL RESEARCH: OCEANS, VOL. 118, 5844–5857, doi:10.1002/jgrc.20403, 2013

Seasonal circulation over the Catalan inner-shelf (northwest Mediterranean Sea)

Manel Grifoll,[1,2] Alfredo L. Aretxabaleta,[3] Josep L. Pelegrí,[4] Manuel Espino,[1,2] John C. Warner,[3] and Agustín Sánchez-Arcilla[1,2]

Received 5 February 2013; revised 12 September 2013; accepted 18 September 2013; published 25 October 2013.

[1] This study characterizes the seasonal cycle of the Catalan inner-shelf circulation using observations and complementary numerical results. The relation between seasonal circulation and forcing mechanisms is explored through the depth-averaged momentum balance, for the period between May 2010 and April 2011, when velocity observations were partially available. The monthly-mean along-shelf flow is mainly controlled by the along-shelf pressure gradient and by surface and bottom stresses. During summer, fall, and winter, the along-shelf momentum balance is dominated by the barotropic pressure gradient and local winds. During spring, both wind stress and pressure gradient act in the same direction and are compensated by bottom stress. In the cross-shelf direction the dominant forces are in geostrophic balance, consistent with dynamic altimetry data.

Citation: Grifoll, M., A. L. Aretxabaleta, J. L. Pelegrí, M. Espino, J. C. Warner, and A. Sánchez-Arcilla (2013), Seasonal circulation over the Catalan inner-shelf (northwest Mediterranean Sea), *J. Geophys. Res. Oceans*, *118*, 5844–5857, doi:10.1002/jgrc.20403.

1. Introduction

[2] The Catalan Sea (CS), located in the Northwest Mediterranean Sea (Figure 1), has atmospheric and oceanographic properties influenced by the semienclosed character of the Mediterranean Sea. Since the Mediterranean is a microtidal environment, the circulation variability in the inner-shelf CS is predominantly affected by storm-induced fluctuations [*Grifoll et al*., 2012] and by forcing mechanisms acting primarily at seasonal scales. Our study aims at identifying and quantifying those mechanisms responsible for the seasonal variability of the velocity field in the inner-shelf of the CS.

[3] The atmospheric seasonal cycle of the NW Mediterranean Sea is characterized by dry summers with well-developed sea breezes and relatively stable atmospheric conditions, transition seasons (autumn and spring) when most of the annual precipitation occurs, and winters characterized by mild temperatures [*Bolaños et al*., 2009]. Most of the regional storms occur in late autumn and through winter, with considerable interannual stability [*Font*, 1990]. These storms are associated with pressure differences between high-pressure systems over the Atlantic or northwest Europe and the low pressure of Mediterranean cyclones over the Gulf of Lion (located north of the Catalan Sea). This cyclonic activity leads to strong north and northeast winds on the Catalan Sea resulting in highly energetic wave events [*Bolaños et al*., 2009] and concentrating its energy at low frequencies (periods over 3 days) associated with synoptic low-pressure systems [*Salat et al*., 1992]. In summer and spring, the dominant wind is southwesterly with the dominant frequencies in the synoptic and diurnal (sea breeze) bands.

[4] The bathymetry on the CS varies from a narrow shelf (<20 km) in the north to a wider shelf (60 km) in the south (Ebro delta region), influencing the hydrodynamic properties of the Catalan coast [*Sánchez-Arcilla and Simpson*, 1992]. The shelf break is located approximately at 150 m depth (Figure 1b). The regional circulation is characterized by the Northern Current [*Millot*, 1999], a quasi-permanent slope current modulated by mesoscale events. These events consist of current meanders and eddies [*Font et al*., 1995] and, in some instances, they reach between the mainland and the Balearic Islands, constituting a source of external variability to the continental shelf [*Font et al.,* 1988]. In addition, *Jordi et al*. [2005] found coastal-trapped wave activity on the Catalan Sea using a conceptual model adjusted to match current observations over the slope.

[5] The freshwater budget in the Mediterranean basin is negative (more evaporation than precipitation) in summer and positive in spring, with a net basin freshwater deficit [*Salat et al*., 2002]. The joint effect of positive heat flux and river discharge, mainly during spring and fall, contributes to water column stratification in the inner-shelf of the Catalan Sea [*Grifoll et al*., 2012]. These conditions, favorable to stratify the water column, are counteracted by intense cooling and wind mixing during fall and winter [*Font*, 1990].

[1]Laboratori d'Enginyeria Marítima (LIM), Universitat Politècnica de Catalunya (UPC), Barcelona, Spain.
[2]Centre Internacional d'Investigació dels Recursos Costaners (CIIRC), Barcelona, Spain.
[3]U.S. Geological Survey, Woods Hole, Massachusetts, USA.
[4]Institut de Ciències del Mar, CSIC, Barcelona, Spain.

Corresponding author: M. Grifoll, Laboratori d'Enginyeria Marítima (LIM), Universitat Politècnica de Catalunya (UPC), Campus Nord, c./Jordi Girona, 1-3, ES-08034 Barcelona, Spain. (manel.grifoll@upc.edu)

2169-9275/13/10.1002/jgrc.20403

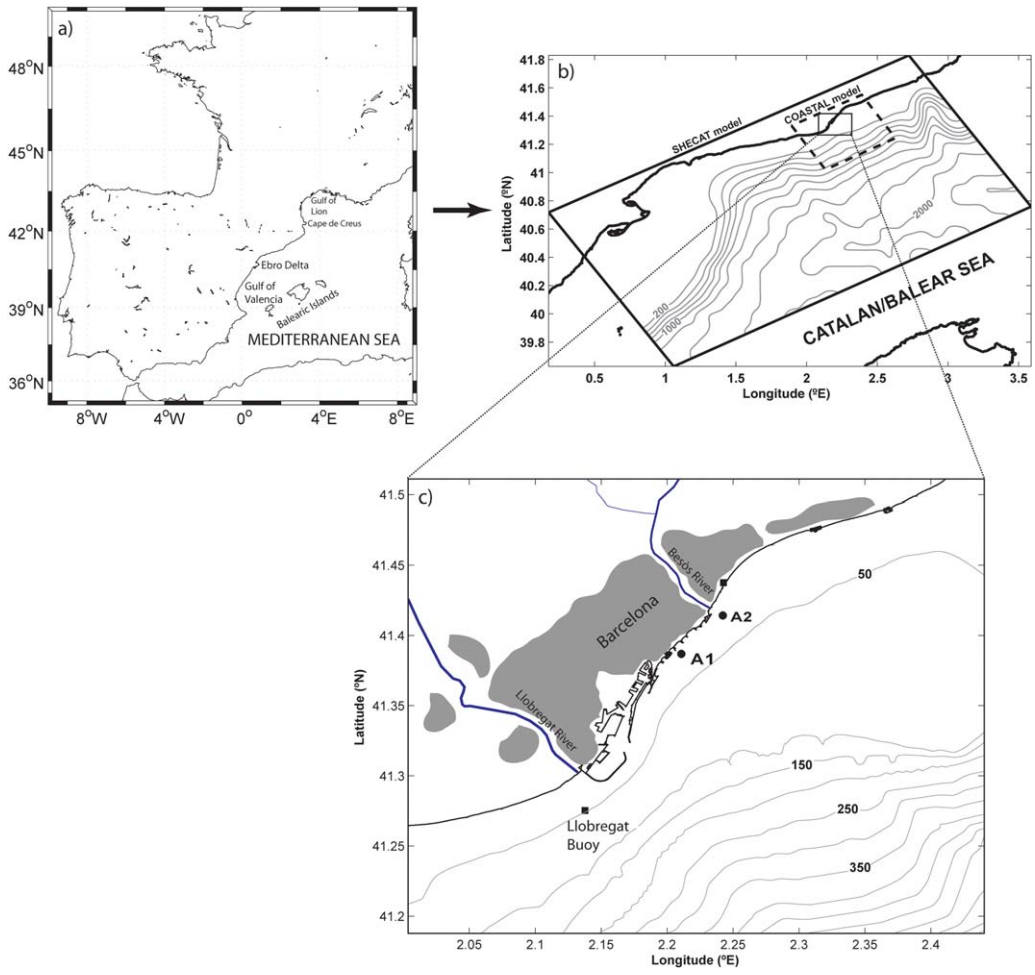

Figure 1. (a) Map of the western Mediterranean with the Catalan Sea. (b) Bathymetry and numerical model domains for the SHECAT and COASTAL configurations. (c) Portion of the Catalan inner-shelf focus of the current study showing the location of the ADCP sensors (A1 and A2) and Llobregat buoy from the XIOM network. The geographic locations mentioned in the text (Cape de Creus, Ebro delta, Gulf of Valencia, Gulf of Lions) are also shown. Urban areas are shown in gray.

[6] The strong seasonality of the Catalan shelf has been described as part of several regional and basin-scale oceanographic studies. For instance, *Millot* [1999] observed sea surface temperature (SST) ranging from 13°C in winter to more than 27°C in summer with a seasonal thermocline present from early spring to late summer. *Petrenko* [2003] also found a noticeable seasonal variability of the slope current in the Gulf of Lion. *Marcos and Tsimplis* [2007] described a water-level seasonal cycle in the Mediterranean Sea. Thus, seasonal variability in water circulation is expected on the CS inner-shelf dynamics, but it yet remains to be properly described.

[7] Several initiatives have been carried out in recent years to increase the level of physical understanding in the Catalan coastal area and, therefore, to contribute to its integral management. First, the development of an observatory network in the Catalan coast has allowed the collection of systematic meteo-oceanographic data in the Catalan shelf area (www.xiom.cat; *Bolaños et al*. [2009]). More recently, in the frame of the European project Field_AC, efficient operational products have been developed. As part of the Field_AC effort, two observational surveys have collected current, wind, waves, hydrographic, and sea-level data in the coastal CS. In contrast with earlier regional studies, mainly in south margin of the Ebro delta [*Font*, 1990; *Salat et al*., 2002], Field_AC has focused on the inner-shelf off the city of Barcelona (Figure 1). *Grifoll et al*. [2012] presented results of one of the observational surveys of the project, describing the water current response to forcing mechanisms in scales ranging from days to weeks. *Grifoll et al*. [2012] found a strong relation between current velocity fluctuation and sea level gradient (synoptic time scales) and local wind (short time scales) during a 1 month period. They also described a small influence of the inertial band due to the dominance of the frictional effects over relatively shallow depths (24 m). To address variations at seasonal scales on the inner-shelf, in this study, we combine water velocity observations with hydrodynamic modeling, neglecting daily and subdaily fluctuations. As the available observations do not cover the entire annual cycle, numerical simulations provide a way to complete the circulation data set and to analyze its relationship with the prevalent forcing mechanisms. The observations are useful not only to calibrate the model results but also to physically sustain

the dynamic patterns revealed by the numerical simulations. The analysis focuses on assessing each term in the depth-averaged momentum balance equations, ranking the importance of the forcing mechanisms during a period that includes both field campaigns: May 2010 to April 2011. This contribution presents, for the first time, the joint results of observational and numerical results to characterize the circulation at seasonal scales over the Catalan inner-shelf.

[8] The paper is organized as follows. Section 2 introduces the observational data used, as well as the numerical model configuration and assessment. Section 3 includes the analysis of atmospheric and river run-off momentum fluxes, and the analysis of the momentum terms in both along- and cross-shelf directions; the seasonal variation is examined at a point where water velocity data is available (24 m depth). The representativeness of the results, in particular the way the current regime responds to different forcing mechanisms and the role played by stratification and regional forcing, is examined in section 4. Finally, we close with a concise description of the seasonal patterns as obtained from the analysis.

2. Observational and Model Data

2.1. Observational Data

[9] The observations were collected in the framework of the Field_AC project during two periods: FIELD1 (from 11 November 2010 to 18 January 2011) and FIELD2 (from 15 March to 15 April 2011). The velocity observations on the inner Catalan shelf were obtained from two Acoustic Doppler Current Profilers (ADCP) moored near the city of Barcelona over the 24 m isobath (stations A1 and A2, Figure 1c), approximately 1 km offshore of Bogatell Beach and the Besos River mouth, respectively. The ADCP used was an AWAC instrument, sampling 25 bin intervals of 1 m at 10 min intervals, with the first cell located 0.4 m from the surface. Additionally, velocity observations from a meteo-oceanographic buoy of the XIOM network were used (Llobregat Buoy). Velocity at the Llobregat location was measured at 1 and 15 m from the surface during 2010 and 2011, unfortunately with significant temporal gaps. This buoy was located at 45 m depth, 17 km south of Barcelona harbor in front of the Llobregat River mouth (Figure 1c), and in the present study is mainly used for model skill assessment.

[10] The dynamics of the Catalan inner-shelf is constrained by the coastal boundary that polarizes the flow along the isobaths, resulting in the spatial scale of the alongshore direction being larger than the onshore/offshore scales [*Allen and Kundu*, 1978; *Lentz and Winant*, 1986; *Lentz and Fewings*, 2012]. The dispersion diagrams of the depth-averaged flow for the FIELD1 and FIELD2 campaigns (Figure 2) reproduce the aforementioned flow alignment. The current variance ellipse angles, given by the principal component analysis (PCA), are well aligned with the local bathymetry.

[11] To characterize the time-averaged flow and its variability, the observations were rotated following the principal angle given by the PCA. This mean depth-averaged flow (Table 1) showed slight differences between both campaigns. During FIELD1, it was statistically indistinguishable from zero, as both mean components were less than the respective standard deviations. During FIELD2, the cross-shelf mean flow remained nonsignificant but a southward alongshore net flow was observed in both ADCPs. For both campaigns and in all ADCPs, the standard deviations in the along-shelf direction, given by the major axis of the ellipse, were between 2 and 6 times larger than the cross-shelf standard deviations (minor axis), confirming the polarization of the flow along the isobaths (Table 1).

2.2. Model and Nesting System

[12] The numerical model used is the Regional Ocean Modeling System (ROMS, *Shchepetkin and McWilliams* [2005]). ROMS is a free-surface terrain-following

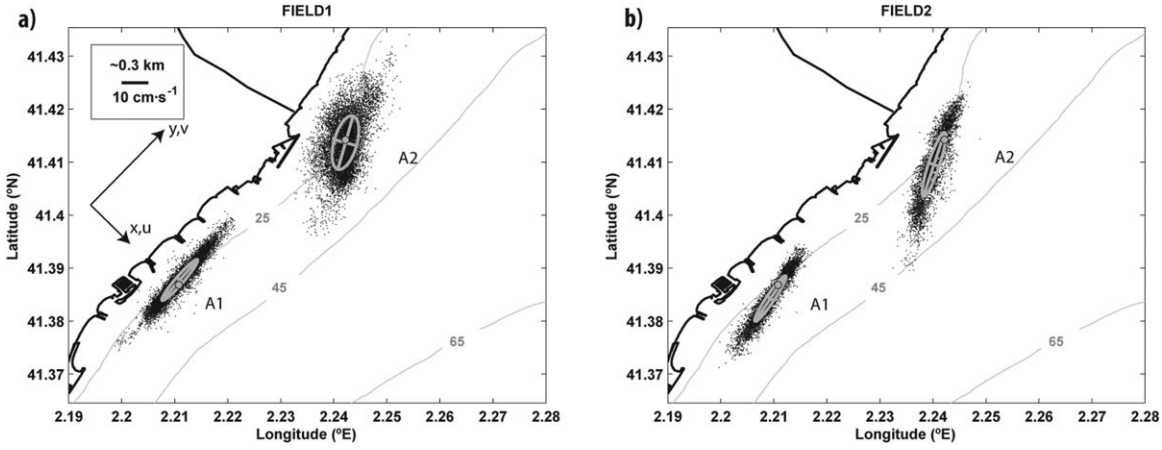

Figure 2. Dispersion diagram and variance ellipses computed from depth-averaged ADCP measurements: (a) FIELD1 (from 11 November 2010 to 18 January 2011), (b) FIELD2 (from 15 March to 15 April 2011). The location of the ADCP moorings is marked with a gray circle. The distance between the circle and the center of the ellipse represents mean velocity. The minor and major subaxes represent the standard deviation. The rotated axes (x, y) with the associated velocity components (u, v) represent the reference system adopted for the momentum balance.

Table 1. Mean Value and Standard Deviation of the Depth-Averaged Velocities at Locations A1 and A2 (cm s^{-1}) as Obtained From Both ADCP Measurements and Model Output

	FIELD1				FIELD2			
	Along-Shelf		Cross-Shelf		Along-Shelf		Cross-Shelf	
	Mean	Std	Mean	Std	Mean	Std	Mean	Std
A1 (z = −24 m) Observed	1.25	10.95	0.13	3.11	−5.25	9.61	0.18	1.54
A1 (z = −24 m) Modeled	0.82	8.35	−0.12	2.82	−7.26	8.63	0.19	1.98
A2 (z = −24 m) Observed	−2.13	11.21	0.14	6.65	−10.08	12.73	0.24	2.06
A2 (z = −24 m) Modeled	−1.68	10.24	0.09	4.54	−11.78	10.73	0.21	1.36

numerical model that solves the three-dimensional Reynolds-averaged Navier-Stokes equations using hydrostatic and Boussinesq approximations. A model grid, with 250 m horizontal resolution, was implemented in front of the city of Barcelona (herein designated as COASTAL model). This grid included 207 × 152 grid cells covering the area where the ADCPs were deployed (Figure 1c). The vertical coordinate had 20 sigma levels, which resolve both surface and bottom boundary layers over the continental shelf.

[13] The open boundaries of the COASTAL model domain were forced by a Mediterranean-scale circulation model [*Tonani et al*., 2009] with a horizontal resolution of 1/16° × 1/16° and 71 unevenly spaced vertical levels, in particular with 20 levels of 3 m resolution near the surface. The Mediterranean model output, part of the forecast/analysis system MyOcean (www.myocean.eu), was available as daily averaged temperature, salinity, sea level, and horizontal velocity fields. The model is a basin-scale Mediterranean Sea model assimilating sea level altimeter data, remotely sensed SST, and in situ observations, forced by remote atmospheric and oceanic pressure gradient forcing among others.

[14] Instead of nesting the coastal domain directly into the MyOcean domain, an intermediate domain (called SHElf CATalan model, SHECAT) was implemented at the scale of the Catalan Shelf (Figure 1) with approximately 1.25 km horizontal resolution. The SHECAT domain was used to properly represent the physical interactions between the general circulation (mainly the Northern Current) and the shelf circulation over the Catalan Shelf, following a nesting ratio of 5 [*Blayo and Debreu*, 2005]. The SHECAT implementation is part of an operational modeling system that ran during a 5 year period (2007–2011). We have chosen the period between May 2010 and April 2011 because it encompassed those times of field measurements. The normal velocities from the SHECAT domain were adjusted to preserve the total mass flux from the coarse grid across the open boundary [*Mason et al*., 2010]. The lateral open boundary conditions consisted of a Flather condition for the 2-D variables and an Orlansky type radiation condition for 3-D fields.

[15] A generic length scale turbulent mixing scheme (*Umlauf and Burchard* [2003], implemented within ROMS by *Warner et al*. [2005]) was used in both COASTAL and SHECAT model domains, with coefficients selected to parameterize the κ-ε scheme [*Rodi*, 1987]. We use the *Kantha and Clayson* [1994] stability function implementation described in *Warner et al*. [2005]. The implementation included fourth order biharmonic Laplacian viscosity and mixing terms in geopotential surfaces for velocity and tracers, respectively, both with constant coefficients of 0.5 m^4 s^{-2}. The bottom boundary layer was parameterized using a log-profile with bottom roughness equal to 0.005 m. Daily atmospheric fluxes (heat and freshwater fluxes, and wind stress) were obtained from the European Centre of Medium-Range Forecast (ECMWF; www.ecmwf.int). Llobregat and Besos river discharge were included in the model as freshwater sources. The runoff data upstream of the river mouths were obtained from monitoring stations managed by the Catalan Water Agency (ACA; www.aca.cat).

2.3. Skill Assessment

[16] Time series of model and observed velocity were compared to assess the skill of the simulations. For this purpose, we used the alongshore velocities of the Llobregat buoy at 1 and 15 m depths (Figure 3) because of their relatively long temporal coverage (from October 9 to 11 April). The model qualitatively reproduces the observed current behavior and its variability while maintaining acceptable statistical skill. At 1 and 15 m the root-mean-square differences were less than 0.16 and 0.12 m s^{-1}, respectively, while the bias was 0.03 m s^{-1} at 1 m and less than 0.02 m s^{-1} at 15 m. For instance, the flow intensification on 12 October 2010, associated with a southeasterly storm lasting several days, was well reproduced in the model for both depths.

[17] The decrease of flow intensity with depth demonstrates that the model was capable of reproducing vertical mixing dynamics, with net momentum transfer from the surface into the deeper layers. The peaks that were not properly reproduced by the simulations occurred during periods with poor wind stress and pressure gradient skill; this was likely caused by limited temporal and horizontal resolution in the atmospheric and remote forcing fields.

[18] Basic statistics of the depth-averaged modeled and observed flows at A1 and A2 are shown in Table 1 for the along- and cross-shelf directions. The mean and standard

Table 2. Cost Function χ of the Model Depth-Averaged Velocities as Compared With Observations

	FIELD1		FIELD2	
	Along-Shelf	Cross-Shelf	Along-Shelf	Cross-Shelf
A1	0.48	0.68	0.37	0.81
A2	0.43	0.52	0.41	0.73

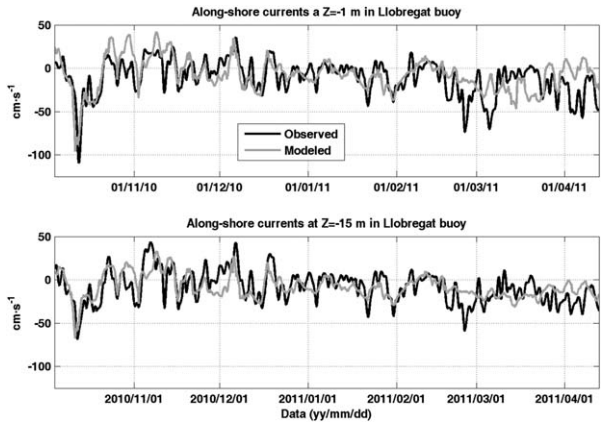

Figure 3. Time series of along-shelf current simulated and measured at the Llobregat buoy location at 1 m (top) and 15 m (bottom) depths.

deviation of the model velocity exhibited good agreement with observed values. Mean water current differences between the FIELD1 and FIELD2 campaigns (e.g., prevalent southwestward flow during FIELD2) were also well reproduced by the model.

[19] The along-shelf and cross-shelf ADCP velocities for A1 and A2, as obtained during FIELD1 and FIELD2 (Figure 4), were graphically compared with the model simulations through Taylor diagrams [*Taylor*, 2001]. This diagram characterizes the similarity between model and observations in terms of their correlation, the centered root-mean-square difference (CRMSD), and the amplitude of their variations (represented by their standard deviations). The model skill improves as the points get closer to the observation reference point in the diagram. In general, the model results showed a good agreement with the observations in the prevalent along-shelf direction, with correlations larger than 0.5 and normalized standard deviations and CRMSD between 0.6 and 1. In the cross-shelf direction, the model results showed slightly larger discrepancies with the observations. In this case, correlations were between 0.4 and 0.6 and the normalized standard deviations and CRMSD were between 0.5 and 1 (Figure 4). The Taylor diagrams also showed the varying skill in the vertical structure of the velocity. In both the along-shelf and cross-shelf directions, the model did best at reproducing the surface layers. During the spring FIELD2 measurements, the model results at A2 displayed some significant discrepancies in the middle part of the water column, likely associated with an increasing stratification that was not properly simulated by the model.

[20] To expand the skill assessment, the cost function [*O'Neill et al*., 2012] for the depth-averaged velocities was calculated in both cross-shelf and along-shelf directions. The cost function (χ) represents a measure of the ratio of model error to the observed variance:

$$\chi^2 = \frac{1}{N\sigma_0^2}\sum_{n=1}^{N}(M_n - O_n)^2 \qquad (1)$$

where O_n and M_n are observed and modeled values, respectively, N is the number of data points and σ_0^2 is the variance of the observations. For the depth-averaged along-shelf direction χ ranged between 0.37 and 0.41, while in the cross-shelf direction it ranged between 0.52 and 0.81 (Table 2). *Holt et al*. [2005] identified 0.4 as the cost function threshold below which the variables are "well-modeled" and 1.0 as the threshold below which the model has predictive skill. Therefore, our model results can be considered adequate to reproduce the flow especially in the along-shelf direction.

3. Results

3.1. Atmospheric Forcing and Land-Sea Fluxes

[21] The annual cycle of meteorological forcing was analyzed in terms of net heat flux and wind stress. The local net heat flux and the wind stress fields, as extracted from the ECMWF products, are shown in Figure 5. The net heat flux variability was concentrated in the annual cycle, being much greater than the variability at other time scales (Figure 5a). The annual cycle in net flux was predominantly associated with the incoming solar radiation, reaching a maximum during summer, which lead to a net heat flux of $\sim$300 W m^{-2}, and to the longwave and latent heat back radiation, peaking during winter and causing a minimum net heat flux of ~ -225 W m^{-2}. The heat budget in this area follows a marked seasonal cycle with relatively small interannual variability [*Castellari et al*., 1998], with downward solar radiation ranging from 80 W m^{-2} (winter) to 360 W m^{-2} (summer), net longwave radiation ranging from 50 W m^{-2} (July) to 100 W m^{-2} (December), sensible heat flux ranging from -10 W m^{-2} (July) to 50 W m^{-2} (January), and latent heat flux from 60 W m^{-2} (July) to 180 W m^{-2} (January).

[22] The low-pass filtered wind stress (cut-off frequency of 0.1 day^{-1}) exhibited significant temporal variability (Figure 5b). Four typical situations may be identified for the period from May 2010 to April 2011, consistent with wind climatology studies in the region [*Font*, 1990; *Bolaños et al*., 2009]. Southerly winds (upwelling-favorable) dominated during the summer season (from mid-May to the end of September). These winds were usually weak and partly modified by sea breeze [*Font*, 1990]. October was characterized by several northeasterly storm events associated with periods of cyclogenesis over the Gulf of Lion, a typically recurrent fall phenomenon [*Bolaños et al*., 2009; *Renault et al*., 2012]. November and December were dominated by "land" winds called Mistral [*Bolaños-Sanchez et al*., 2007]. Finally, during the period of January-April, northeasterly winds (downwelling-favorable) were prevalent but with high variability in wind direction.

[23] The Llobregat and Besos river discharge time series were consistent with the Mediterranean climate (Figure 5c). Two high-flow regimes, associated with wet seasons (spring and autumn), were observed between the low-flow conditions that occur during the dry seasons (summer and winter). The seasonal cycle was more evident in the Llobregat River as it has a larger mean flow consistent with its greater catchment area [*Liquete et al*., 2009].

3.2. Along-Shelf Analysis

[24] The biweekly-mean depth-averaged along-shelf currents, observed during both surveys at A1, are included in

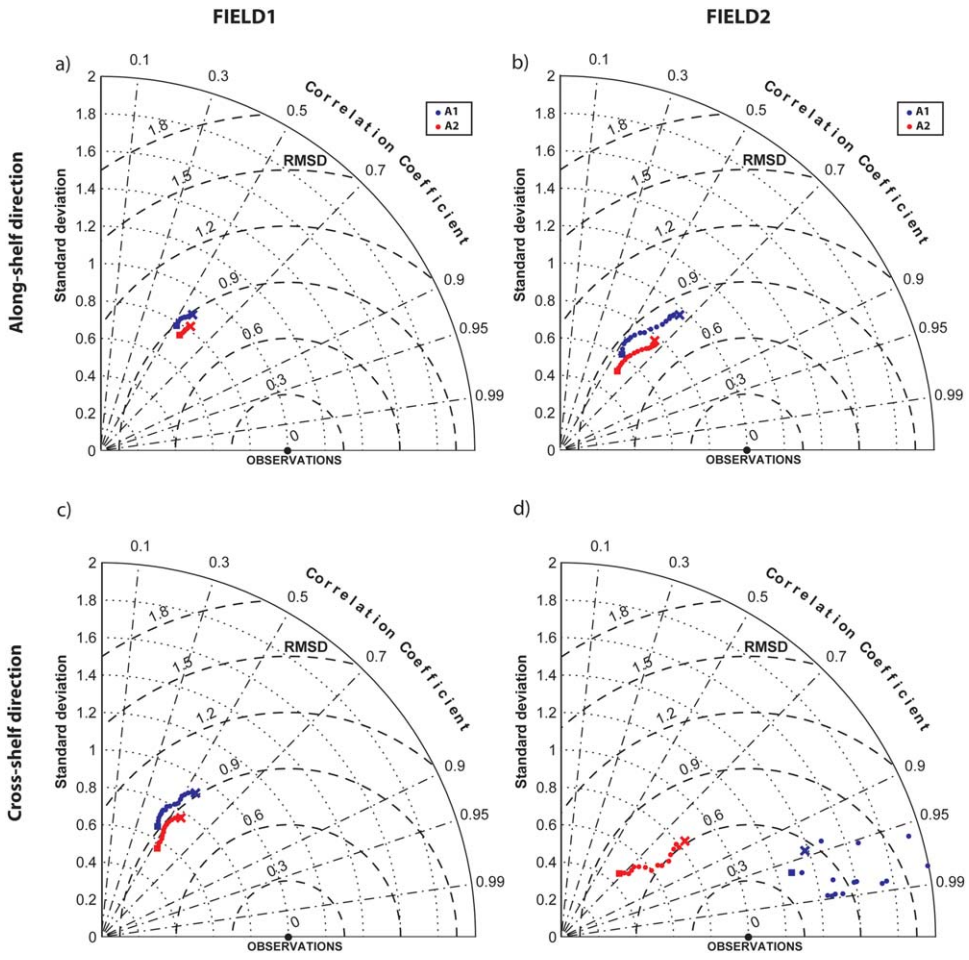

Figure 4. Taylor diagram comparing the statistics of observations and model results in the along- and cross-shelf directions corresponding to (a, c) FIELD1 and (b, d) FIELD2 experiments. The standard deviation is normalized with respect to the observations; units of root-mean-square difference (RMSD) are standard deviations. The blue and red points correspond to the results at locations A1 and A2, respectively. The square and crosses, respectively, represent the bottom and surface layers.

Figure 6. The along-shelf currents were near zero during FIELD1 (late-fall and winter) and southwestward during FIELD2 (spring). When observational data were not available, then model output at A1 was used for the analysis. Maximum along-shelf velocities were estimated for March and April 2010. The standard deviation during these 2 months, as computed using model outputs (Figure 6), was smaller than the mean flow, suggesting a limited occurrence of flow reversals. During the rest of the year, the flow temporal variability was larger than the mean, suggesting that northwestward and southeastward flow reversals were common.

[25] Assuming hydrostatic flow and neglecting the nonlinear terms, wind-wave momentum fluxes, and baroclinic contributions to pressure gradient, the along-shelf depth-averaged momentum balance may be written as

$$\frac{\partial v}{\partial t} + fu = -g\frac{\partial \eta}{\partial y} + \frac{1}{H\rho_0}\left(\tau_{ys} - \tau_{yb}\right) \qquad (2)$$

where v and u are the along and cross-shelf depth-averaged velocities, respectively, f is the Coriolis parameter, η is the sea-level, ρ_0 is the reference density, H is water depth, and τ_{ys}, τ_{yb} are the sea surface (wind) and bottom along-shelf stresses, respectively. The terms in equation (2), from left to right, are local acceleration, Coriolis force, barotropic pressure gradient, and the volume forces associated to the wind and bottom stresses. The size of the neglected terms (e.g., nonlinear or baroclinic pressure gradient terms) is likely important in shorter than monthly time scales [*Grifoll et al*., 2012] and for specific areas. For example, the wind-wave momentum flux only becomes predominant in the proximity of the surf zone [*Lentz et al*., 1999; *Lentz and Fewings*, 2012].

[26] When enough data were available, the Coriolis, barotropic pressure gradient, and frictional terms were estimated using observations, as in *Grifoll et al*. [2012]. Differences in wind and bottom stress momentum terms were observed between FIELD1 (fall/winter) and FIELD2 (spring). The pressure gradient force (i.e., $-g\ \partial\eta/\partial y$) was estimated only during FIELD2 because of the availability of consistent sea-level data for the Catalan Sea only during that period. The Coriolis term had similar magnitude during

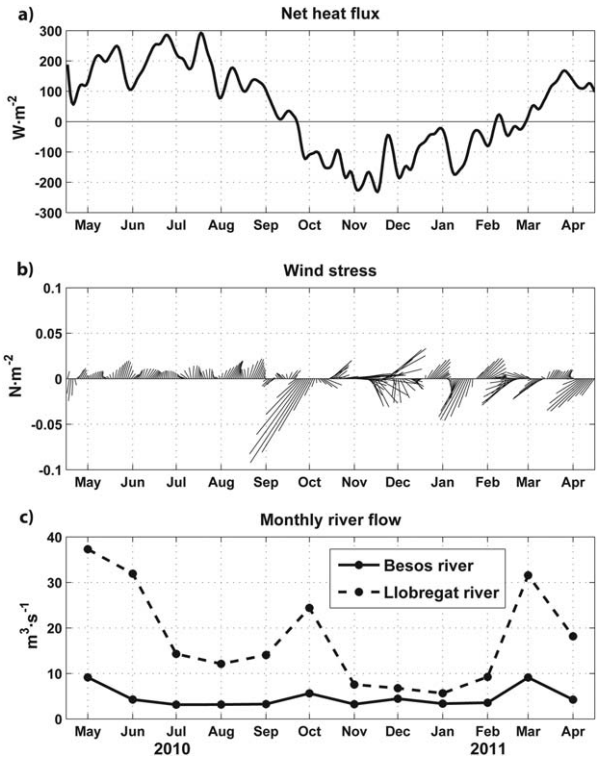

Figure 5. Low-pass filtered (cut-off period of 10 days) (a) net heat fluxes and (b) winds from ECMWF. (c) Monthly-mean discharge for the Llobregat and Besòs rivers. Tick marks indicate the middle of the month.

both periods, being much smaller than the other terms. Monthly averaged model outputs were used to investigate the temporal variability of the momentum terms for the entire seasonal cycle. Model-derived momentum terms were consistent with the momentum terms estimated from observations. The model barotropic pressure gradient was computed by differentiating the sea level in contiguous computational grid cells. Bottom frictional and Coriolis terms were computed from model velocity fields and the wind stress term from atmospheric forcing.

[27] The temporal evolution of the momentum terms (Figure 6b) reveals that along-shelf pressure gradient and wind stress were the dominant forces in the momentum balance. The size of the bottom friction term was substantially smaller than the pressure gradient and wind stress except during spring. The acceleration term (not shown) was at least one order of magnitude smaller than the Coriolis term at monthly time scales. The largest term corresponded to the pressure gradient force which, except during October, was always negative (in the same direction as the flow). During the summer months, the size of the pressure gradient term was relatively constant, but during the rest of the year it exhibited sizeable variability. The role of the along-shelf wind stress varied throughout the year but generally opposed the flow. Positive wind stress was predominant during summer (June-September, due to southwesterly winds, Figure 5), opposing the pressure gradient force. During October, the period with highest storm activity, the wind stress acted in the same direction as the flow and opposed the pressure gradient force. During November and December, the wind stress (dominated by westerly winds) increased in magnitude and opposed a reinforced pressure gradient force. During March and April, both the wind stress (northeasterly winds) and the pressure gradient force had the same direction, causing the southwestward currents to reach a maximum during this period.

[28] The bottom stress term varied significantly along the year, with low and moderate magnitudes during most of the year except during March and April when bottom stress became dominant. The Coriolis term was small during the entire year so that its influence in the momentum equation was only noticeable when the other terms were small (e.g., July). The secondary role of the Coriolis term on the along-shelf momentum balance was consistent with the strong along-shelf flow polarization. The size of the momentum terms, as calculated using either the numerical model or the observations, was similar, therefore confirming the robustness of our analysis.

[29] The residual in the along-shelf momentum balance included local flow accelerations and nonlinear effects occurring at time scales shorter than monthly periods, therefore being partially compensated when calculating monthly averages. The size of the acceleration and nonlinear terms for periods of 3–5 days was as large as $\pm 5 \times 10^{-6}$ m s^{-2}, as estimated from observations [*Grifoll et al*., 2012], but when averaged over a 3 week period the local acceleration reduced to 0.2×10^{-6} m s^{-2}. This value was of the same order as the residual in the along-shelf momentum balance, its root-mean-square (RMS) value being 0.3×10^{-6} m·s^{-2}.

[30] Another term included in the residual is the baroclinic pressure gradient term. In the along-shelf direction, this baroclinic term may be evaluated from model output as

$$\frac{\partial p_{BAROC}}{\partial y} = -\frac{1}{H\rho_0}\frac{\partial}{\partial y}\int_{-h}^{\eta} g\rho z \mathrm{d}z \qquad (3)$$

[31] With the help of this last equation, the calculated average monthly value in the along-shelf direction was 0.1×10^{-6} m s^{-2}, consistent with estimates from observations in the CS [*Grifoll et al*., 2012].

[32] The monthly-mean modeled along-shelf vertical velocity profiles exhibited substantial differences between the summer months and the rest of the year (Figure 7). The vertical profiles were consistent with the depth-averaged velocities (Figure 6a), exhibiting larger along-shelf velocities during spring. During summer (June to September), the velocity was maximum in mid-water depths and approached zero near the sea bottom, with surface reversals in June and September. The vertical profiles were fairly homogeneous during fall and winter with almost inappreciable differences between the motion in the upper and lower layers (particularly November to February). March, April, and May exhibited moderate vertical gradients with minimum velocities near the bottom. These spring months showed along-shelf vertical profiles with larger surface velocities than the rest of the year. The observed vertical profiles (not shown) revealed a similar along-shelf velocity structure, with maximum flow during spring.

3.3. Cross-Shelf Analysis

[33] The cross-shelf depth-averaged momentum balance can be written considering local acceleration, Coriolis

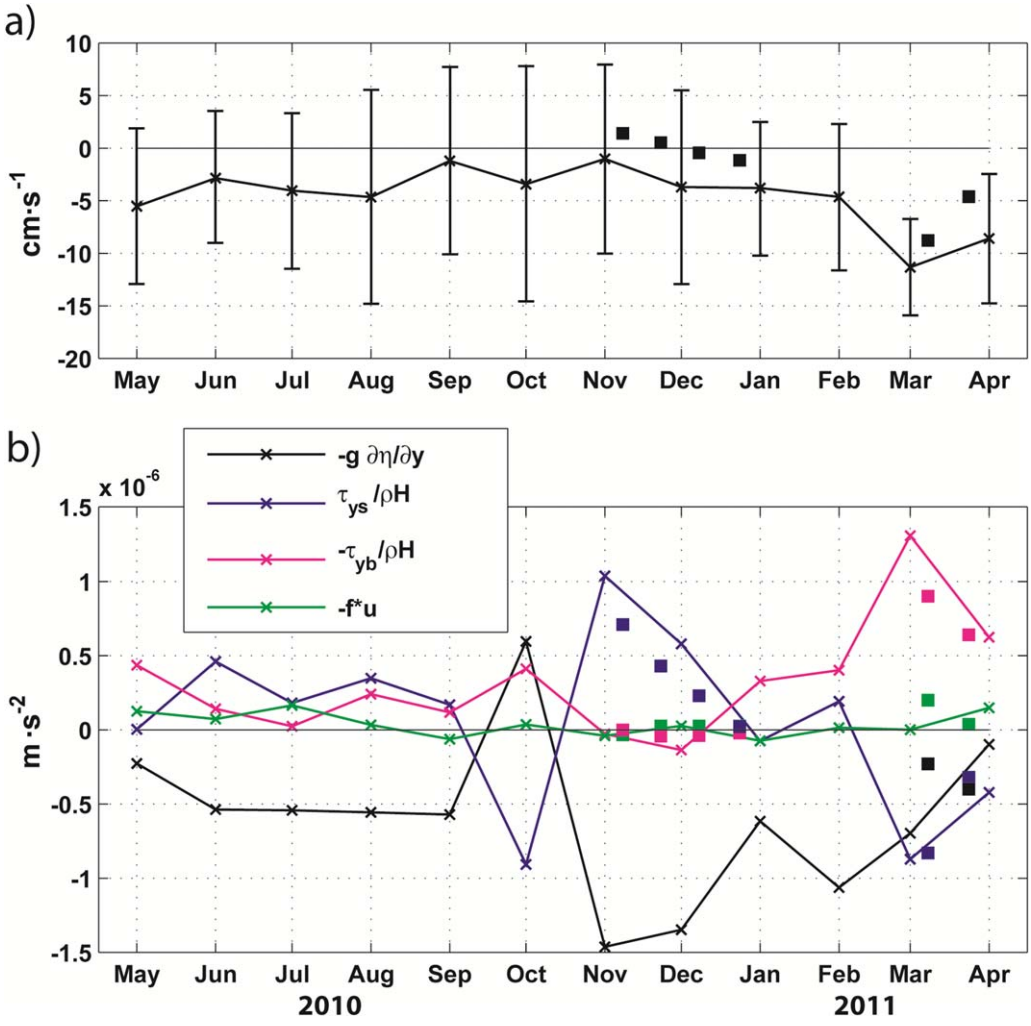

Figure 6. (a) Mean and standard deviation of the depth-averaged along-shelf velocity at A1. Observations, shown as squares, are 2-week averages. Monthly averaged model outputs, shown as x symbol, are also included. (b) Evolution of the along-shelf momentum terms at location A1 as estimated with data (squares) when possible and as computed with the model. The direction is consistent with the axis shown in Figure 2. The average residual is 0.3×10^{-6} m s^{-2}. Tick marks indicate the middle of the month.

force, barotropic cross-shelf pressure gradient, and frictional forces as follows:

$$\frac{\partial u}{\partial t} - fv = -g\frac{\partial \eta}{\partial x} + \frac{1}{H\rho_0}(\tau_{xs} - \tau_{xb}) \qquad (4)$$

[34] Momentum fluxes due to waves may be significant at depths of 25 m during storm events, but at monthly timescales they may be neglected because the average wave climate of the Mediterranean Sea is not highly energetic [*Bolaños et al*., 2009]. Figure 8 shows biweekly mean momentum terms as estimated from observations; note that the available sea-level data did not allow the estimation of the cross-shelf pressure gradient. The Coriolis force and likely the cross-shore pressure gradient force were the dominant terms during FIELD1 and FIELD2, while bottom and wind stresses were second-order terms.

[35] Monthly-averaged model output is used to complement field data (Figure 8). According to these results, the prevalent momentum balance during the entire year was between the Coriolis force and the cross-shelf pressure gradient force, i.e., the along-shelf current drives the cross-shore velocity (equation (4)) which, because of the coastal constraint, induces a cross-shelf elevation gradient until a cross-shore geostrophic is attained. Both terms were highly correlated and larger than the frictional terms and at least three orders of magnitude greater than the acceleration term (not shown). The wind stresses were only noticeable when the pressure gradient and Coriolis terms were small. For instance, November was characterized by energetic "land" winds that increased the relative importance of the surface frictional term in the momentum balance until reaching the same magnitude as the Coriolis term. The cross-shelf bottom stress term was an order of magnitude smaller than the two dominant terms year round. The residual of the cross-shelf momentum balance was small in comparison to the prevailing geostrophic balance (RMS of the residual term was 0.9×10^{-6} m s^{-2}). The residual also included baroclinic effects, which are estimated as

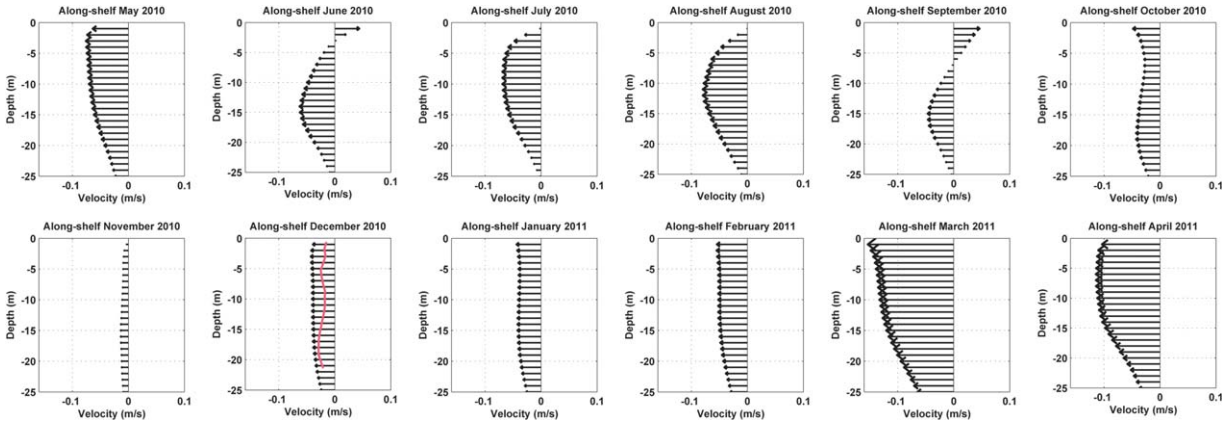

Figure 7. Monthly-mean vertical profiles of along-shelf current velocity modeled at location A1. The observed profile during December 2010 (the only time with data available during the entire month) is also plotted (in red). The direction is consistent with the axis shown in Figure 2.

$$\frac{\partial p_{BAROC}}{\partial x} = -\frac{1}{H\rho_0}\frac{\partial}{\partial x}\int_{-h}^{\eta} g\rho z \mathrm{d}z \tag{5}$$

[36] The average monthly baroclinic term in the cross-shelf direction was 1×10^{-6} m s^{-2}. There was an enhanced baroclinic contribution in the proximity of the plume during periods of large river discharge, approximately 10 times larger than during periods of low discharge. These values were consistent with baroclinic terms as estimated from observations in the CS [*Grifoll et al*., 2012]. River plume dynamics was not further considered as it falls below the spatial scales of interest for our study.

[37] The vertical profiles of the cross-shelf velocity (Figure 9) exhibited higher variability than the along-shelf profiles (Figure 7), although their amplitude was substantially smaller because of the coastal boundary constraint. During those months with persistent cross-shelf winds the profiles displayed the largest vertical structure. In November/December, when the Mistral land winds dominated, the vertical profiles were characterized by surface layer flow in the same direction as the wind and opposite subsurface velocities. In this case, the evident inverse relationship between cross-shelf wind and bottom stress was consistent with a two-layer cross-shelf flow structure driven by cross-shelf wind forcing [*Fewings et al*., 2008]. This suggests that cross-shelf winds may drive significant cross-shelf circulation in the inner shelf, when the top and bottom boundary layers overlap [*Tilburg*, 2003]. In January and March, the velocity profile was reversed, with onshore flow in the upper layer and offshore interior flow, reflecting downwelling conditions consistent with the observed along-shelf northeasterly winds (Figure 5b). This situation was similar to typical mid-shelf circulation patterns, where the surface and bottom layers do not overlap [*Fewings et al*., 2008]. The dynamics at 24 m depth responded to local forcing but it could also be possibly affected by along-shelf divergences that generated onshore/offshore fluxes. Thus, the changing conditions at the study location probably cause the area to behave as "inner-shelf" during times when rotational effects were small (e.g., cross-shelf winds driving cross-shelf transport) and "mid-shelf" during times when rotation was more important (along-shelf winds driving cross-shelf transport). Also, the small influence of wind stress was limited to the uppermost layers and likely the vertical profiles responded to weak upwelling/downwelling processes that were not captured at monthly scales.

4. Discussion

[38] Seasonal changes in the inner-shelf circulation depend on the relative importance of the predominant forcing mechanisms in the momentum balance. The most common along-shelf flow was southwestward but flow reversals occurred during most of the year. Except October, March, and April, the prevalent southwestward flow was in the same direction as the dominant along-shelf pressure gradient force. During October, the along-shelf wind stress opposed the pressure gradient force and the resulting flow. This negative correlation between wind and pressure gradient force was presumably associated with the local response of the flow to spatial variations in forcing and bathymetry [*Lentz and Fewings*, 2012], as reported for many continental shelves (e.g., Northern California Shelf, *Lentz* [1994]; Caribbean coast of Colombia, *Maza et al*. [2006]; West Florida Shelf, *Liu and Weisberg*, [2005]). In these cases, the along-shelf wind stress is the dominant driver of the along-shelf current on the inner-shelf and bottom friction, pressure gradient and the Coriolis force are consequences of the wind stress forcing [*Liu and Weisberg*, 2005]. The inner-shelf geometry, relative to the regional wind regime, defines the resulting momentum balance.

[39] In some cases, along-shelf pressure gradient is associated with a nonlocal origin [*Hickey*, 1984; *Lentz and Winant*, 1986]) and the negative correlation between pressure gradient force and wind stress can disappear. During March and April 2011, wind stress and pressure gradient force were not anticorrelated (both have the same along-shelf direction) and therefore bottom stress played a greater role (Figure 6b). In this case, a remote or nonlocal forcing is likely responsible for the observed pressure gradient and results in low correlations with local wind. During spring conditions (from March to May), the along-shelf flow

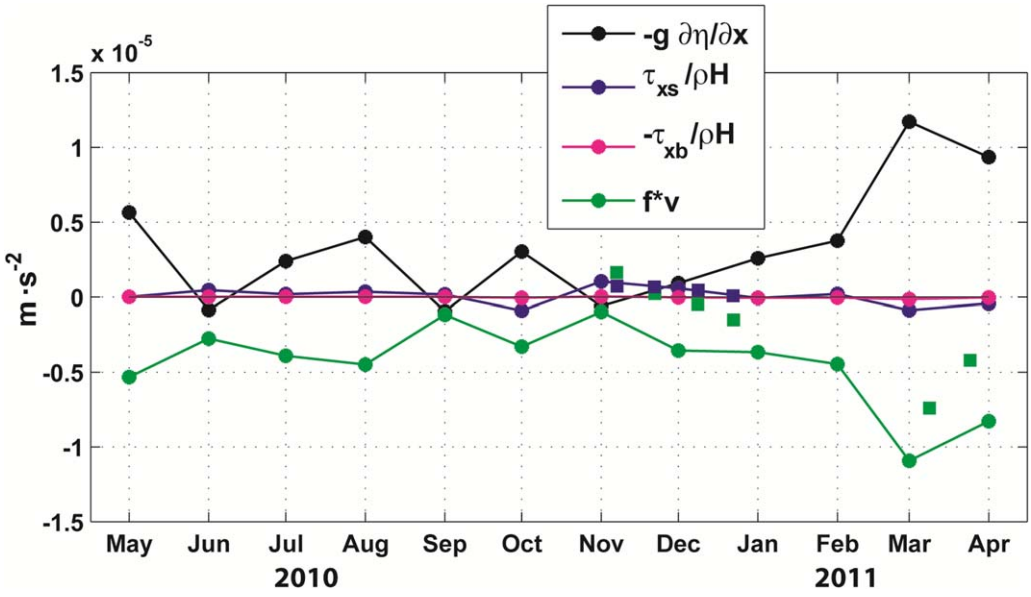

Figure 8. Evolution of the cross-shelf momentum at location A1 as estimated with data (squares) when possible and as computed from the model. The average residual is 0.9×10^{-6} m s^{-2}. Observations, shown as squares, are 2-week averages. Monthly-averaged model outputs, shown as circles, are also included. Tick marks indicate the middle of the month.

reached maximum values and the resulting momentum balance was substantially different from the rest of the year. This spring behavior reflects the existence of nonlocal processes that lead to along-shelf pressure gradients as reported in the Oregon [*Hickey*, 1984] and California [*Lentz and Winant*, 1986; *Hickey et al*., 2003] shelves.

[40] The regional surface circulation of the Catalan/Balearic Sea is characterized by the presence of the Northern Current running southwest from the north until the center of the Gulf of Valencia (Figure 1). *Mason and Pascual* [2012] examined the seasonal sea level anomaly fields from 18 years of the 1/8° AVISO merged Mediterranean data. Their results showed that in the proximity of our study area, off the northern end of the city of Barcelona, the seasonal Northern Current intensifies during winter-spring and weakens in summer. In this sense, weekly AVISO Mediterranean data can be used to estimate the changes in absolute dynamic topography (ADT) values for our period of interest (May 2010 to April 2011). The 1/8° resolution represents about 10 and 14 km in the zonal and latitudinal directions off the city of Barcelona so that in some locations the shelf was barely resolved. Despite the resolution deficiency in the inner shelf, ADT could be useful to understand how the regional dynamics may have affected the shelf circulation (Figure 10).

[41] A predominant cyclonic gyre, formed by the Northern and Balearic Currents, was present year-round. High ADT values along the Catalan shore and further south, in the Gulf of Valencia, may usually be tracked upstream into the Gulf of Lion. In the proximity of the Catalan shelf, the

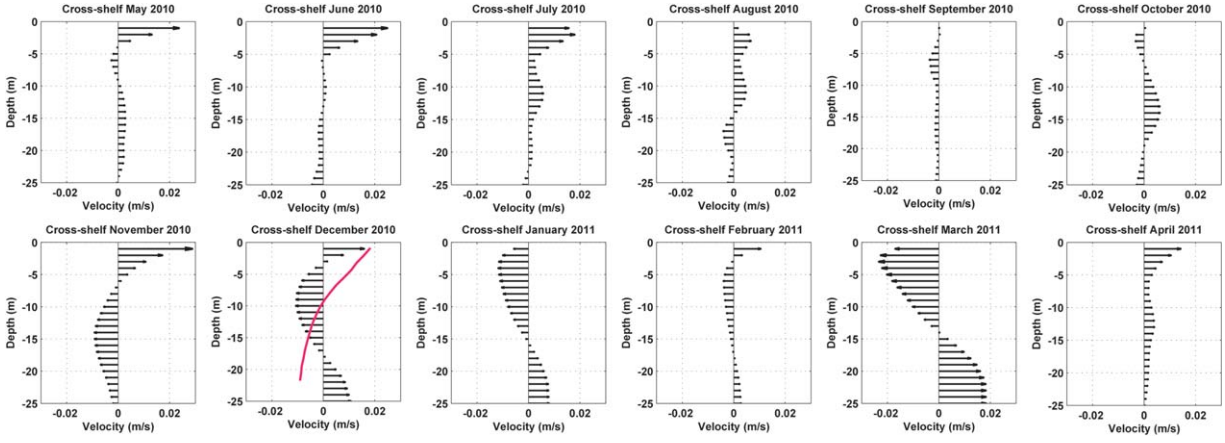

Figure 9. Monthly-mean vertical profiles of cross-shelf current velocity modeled at location A1. The observed profile during December 2010 (the only period with observational data available for an entire month) is also plotted (red line). The direction is consistent with the axis shown in Figure 2.

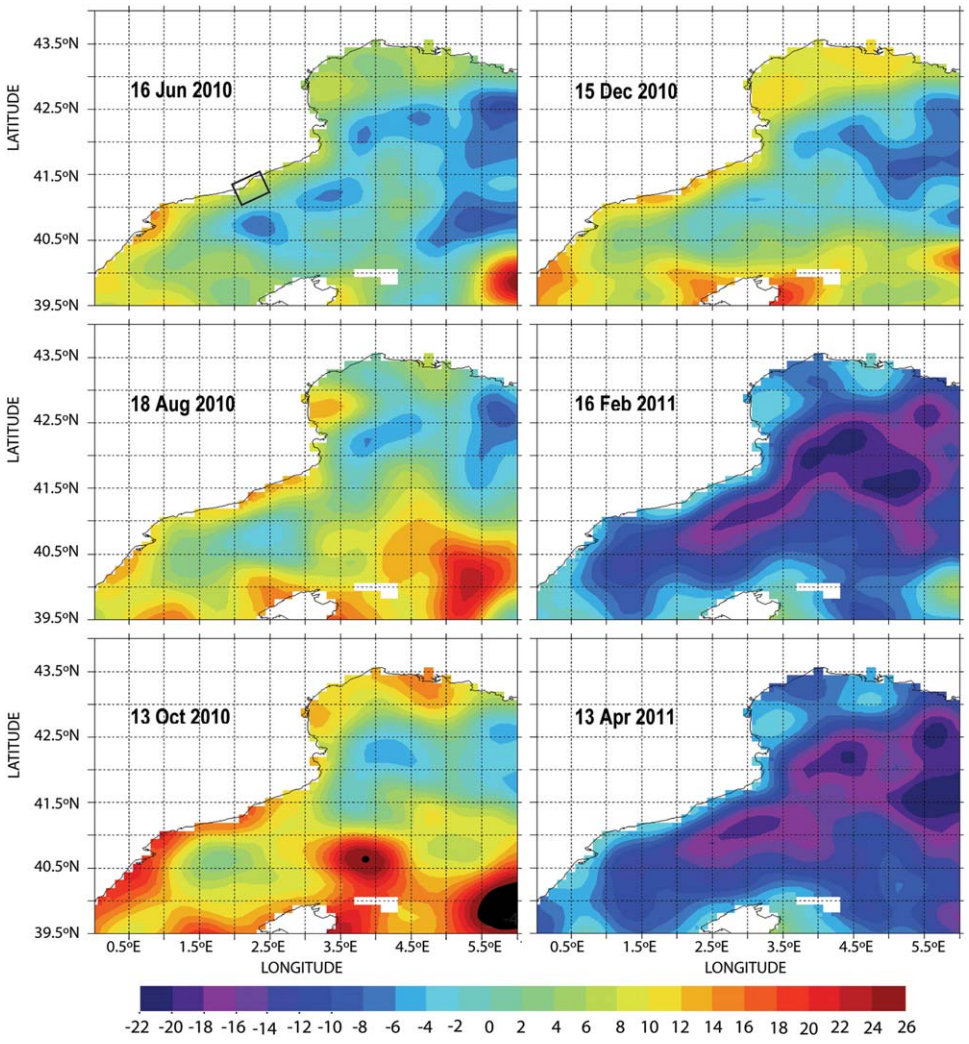

Figure 10. Absolute dynamic topography (values in centimeters) for the whole Catalan Sea, approximately every 2 months, during our study period. Note the scale has 2 cm intervals between −16 and 16 cm, and one additional 10 cm interval beyond these two values. The figures have been obtained using the DUACS interactive system in the AVISO web page, www.aviso.oceanobs.com. The top-left figure shows the area of interest.

cross-shelf pressure gradient increased slowly between June 2010 and October 2010, remaining relatively high between October 2010 and December 2010 and decreasing between December and April 2011. In October 2010, an isolated ADT high, a mesoscale feature with diameter close to 100 km, was located offshore at the latitude of the city of Barcelona and appeared to temporarily break the predominant offshore cyclonic regional circulation. A comparison of Figure 10 with Figures 6–8 reveals the important role of the along-shelf wind in modulating the along-shelf pressure gradient. Figure 7 shows that the along-shelf flow weakened in September 2010, with the along-shelf pressure gradient force being balanced by the wind stress (Figure 6), and completely changed in October 2010 in comparison to previous months.

[42] October was dominated by intense winds from the northeast, which drove a moderate surface south-westward current and caused a local inversion in the pressure gradient. This was a spatially limited feature as the currents were small and had no possibility of draining the high water elevations found along the coast, as reflected by the ADT distribution during 13 October (Figure 10). The mesoscale feature located off Barcelona may have been the outcome of these dynamics, being responsible for temporarily closing the cyclonic regional Northern-Balearic gyre off Barcelona (Figure 10); at this time, the location off Barcelona acted as a stagnation point for offshore water flow. In March and April 2011, high south-westward flow probably drove the rapid decrease in ADT within coastal and deep waters of the Gulf of Lion (Figure 10), consistent with the nonlocal origin of the along-shelf pressure gradient.

[43] The storm during 10–15 October was a typical event originated by a cyclogenesis in the Northwest Mediterranean Sea, favored by orographic effects and intensified by the air-sea contrast [*Jansá*, 1994]. Due to their frequency, duration, and intensity, cyclogeneses play an important role in the climate of the region [*Lionello et al*., 2007], causing extreme wind and wave events [*Bolaños-Sanchez et al*.,

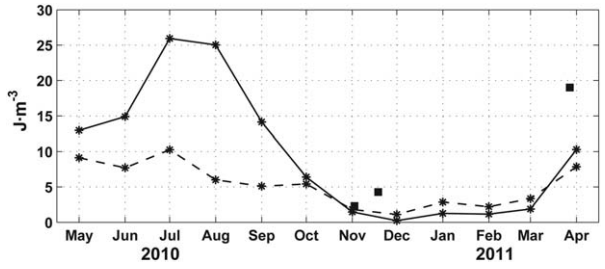

Figure 11. Monthly depth-averaged mean (solid line) and standard deviation (dashed line) ϕ values as obtained from the model output (asterisks) and the CTD surveys (squares) at 24 m depth.

2007]. The number, timing, and intensity of the events generated over sea during fall and winter may change greatly from 1 year to another [*Lionello et al*., 2007].

[44] To analyze the stratification in the water column, the potential energy anomaly (ϕ) was obtained from CTD measurements (Figure 11) during fall (16 November 2010 and 2 December 2010, during FIELD1) and spring (10 April 2011, during FIELD2). The anomaly quantifies the deficit in potential energy (PE) due to stratification compared to the fully mixed water column and is computed as

$$\phi = \frac{PE_{mixed} - PE}{H} = \frac{1}{H}\int_{-h}^{\eta} (\overline{\rho} - \rho) g z \mathrm{d}z \qquad (6)$$

where $\overline{\rho}$ is the vertically averaged density and PE_{mixed} is the potential energy for fully mixed water conditions. The seasonal cycle for ϕ may be inferred from model output. The results show maximum values during July and August (25 J m^{-3}) and minimum values during winter ($\sim$0 J m^{-3}), associated with well-stratified and well-mixed conditions, respectively. The maximum stratification was observed in July and corresponded with a slope Burger number (defined as $S = \alpha N/f$, where A is the bottom slope, N is the buoyancy frequency, and f is the Coriolis parameter) of $S = 1.7$. During weak stratification conditions (e.g., December), the Burger number was 0.17. The S value under stratification conditions was relatively high when compared with other shelves [*Lentz and Chapman*, 2004] due to the steepness of the Catalan shelf (note that the shelf width in CS is relatively narrow, $\sim$ 20 km).

[45] River discharge peaks (May, October, and March) were not synchronous with maximum ϕ values, suggesting that the seasonal ϕ cycle was primarily controlled by heat flux at monthly scales. However, high ϕ standard deviations were observed during months of peak river discharge, implying that the main effect of the rivers was to increase the stratification variability. In consequence, high heat flux combined with mild winds resulted in increased thermal stratification in the water column, consistent with the analysis of potential energy changes presented in *Grifoll et al*. [2012]. Directly influenced by stratification, the vertical along-shelf velocity profiles (Figure 7) exhibit a multilayer structure during summer, consistent with the increased ϕ. Stratification tends to decouple the velocities at depth, often resulting in decreased velocities or flow reversals. Such strong decoupling was only obvious in the across-shelf currents (Figure 8), which were far from geostrophic balance (Figure 6), therefore pointing at the importance of internal friction during highly stratified conditions.

[46] Cross-shelf dynamics were dominated by the geostrophic balance between Coriolis acceleration and cross-shelf pressure gradient force. This balance is common in open-ocean conditions and also in shelf environments with depths similar to our study area (e.g., *Lee et al*. [1989] in South Atlantic Bight, USA; *Lentz et al*. [1999] in North Carolina inner-shelf, USA). The monthly evolution of the cross-shelf balance was affected by the along-shelf current variability. For example, large along-shelf velocities during March 2011 yielded cross-shelf terms larger than during September or November 2010, when along-shelf velocities were small. For the latter situation, the frictional forces played a significant role because of the decreased prevalence of the geostrophic balance, for example, because of the presence of "land" winds (November 2010). Overall, the seasonal cycle in the cross-shelf direction was less evident than in the along-shelf because of the dominance of the geostrophic equilibrium.

[47] The observed and modeled circulation patterns during the March 2010–April 2011 period are likely representative of the seasonal variability within the inner-shelf of the CS. A clear seasonal pattern, consistent with the Mediterranean climate, appears in all forcing mechanisms: continental run-off [*Liquete et al*., 2009], wind variability [*Font et al*., 1990], storm events [*Bolaños et al*., 2009; *Renault et al*., 2012], sea-level [*Marcos and Tsimplis*, 2007], evaporation minus precipitation and heat fluxes [*Castellari et al*., 1998]. Preliminary results suggest that interannual variability in the inner-shelf is relatively small when compared to the size of the seasonal cycle described herein (not shown). Reliable interannual observations are needed to support such estimates. It is possible that subseasonal fluctuations, such as the frequency of short-term river and wind events, may drive some annual variability, but this analysis is left for future studies.

[48] Previous studies on the Catalan Sea have suggested that in the outer shelf and slope the subinertial motions of the along-slope flow are affected by the shelf-slope front [*Font et al*., 1990; *Salat et al*., 2002]. The Northern current flows southwestward in geostrophic balance, associated with the shelf-slope front [*Millot*, 1999] and characterized by small frictional influences. Our results underscore the relevance of the cross-shelf geostrophic balance even within the inner shelf but also point at the existence of significant along-shelf frictional influences. The frictional terms may be responsible for a lag of correlation between inner- and outer-shelf currents, with local changes in the along-shelf direction.

[49] Numerical model outputs allow the computation of the momentum terms during the entire year ensuring physical consistency among the terms. The size of the momentum terms calculated using model outputs were similar to the estimates using observations (Figures 6b and 8). *Grifoll et al*. [2012] highlighted the uncertainties when estimating some of the momentum terms in the CS from observations. For example, the along-shelf pressure gradient was estimated in FIELD2 from two sea-level gauge stations

separated by 100 km. *Hickey* [1984] noted that common sea-level differences in the along-shelf are of the order of a few centimeters (for distances of the order of the external Rossby radius), which means that the uncertainty in the observations may lead to misrepresentations of the barotropic pressure gradient term. *Fewings and Lentz* [2010] also highlighted the small horizontal scale that characterizes the across-shelf sea level gradient, potentially resulting in underestimates when using observational data. In our investigation, we have relied upon properly assessed numerical model implementations to complement observational data, providing a successful combination for inner-shelf research.

[50] The resulting along-shelf momentum balance, with dominant pressure gradient and frictional forces, is highly sensitive to total water depth. The inner-shelf, here characterized by a location at 24 m depth, acts as a transition between the near-shore, where the balance presumably would be between the surface gravity wave stress and bottom friction [*Lentz*, 1994; *Fewings and Lentz*, 2010], and the outer-shelf, where the cross-shore geostrophic balance (pressure gradient and Coriolis force) is dominant [*Winant et al*., 1987; *Fewings et al*., 2008]. This behavior is common to many shelves where field data at comparable depths yield similar momentum balances [*Lentz et al*., 1999; *Maza et al*., 2002; *Liu and Weisberg*, 2005]. Additionally, the orography of the region is characterized by river valleys (e.g., Besos and Llobregat) that increase the spatial variability of the wind field (wind jets) with a potentially large influence on hydrodynamics [*Schaeffer et al*., 2011]. Determining the depth where wind waves or rotational effects are important is left for future studies on the spatial variability of the inner-shelf dynamics.

5. Summary and Conclusions

[51] Our analysis represents a first interpretation of the seasonal dynamics on the Catalan Sea inner-shelf based on observations and numerical model results. It has focused on a detailed analysis of field and numerical data from one single location (24 m depth), where current observations allowed model verification. A clear seasonal along-shelf pattern is found. During summer, the pressure gradient force dominates the momentum balance counteracting the surface momentum introduced by wind stress. Significant vertical shear in the water column is also observed, consistent with relatively large stratification caused by heat fluxes and, to a smaller degree, by rivers discharge. Fall may be considered as a transitional period, generally characterized by its instability. For instance, October 2010 was dominated by a typical storm with easterly winds resulting in a predominant along-shelf force balance between wind stress and pressure gradient. These conditions exhibit the largest interannual variability, as the timing and number of storms is concentrated during the fall and winter seasons but may vary significantly from year to year. During winter, the atmospheric forcing is characterized by energetic winds with an important "land" component. The along-shelf pressure gradient force dominates the momentum balance with along-shelf winds opposing the flow. Weak stratification and homogeneous vertical velocity profiles, due to cooling and low river discharge, allow the increased wind energy to mix the entire water column. Finally, spring is characterized by highly variable winds. There is an intensification of the along-shelf velocity due to the combined effect of the pressure gradient force and along-shelf winds that is partly counteracted by bottom friction. Our analysis suggests that during spring the pressure gradient is mostly remote, as shown by the regional distribution of dynamic topography. Also, vertical shear and stratification develops due to river discharge and the gradually increasing heat flux.

[52] Overall, we may conclude that, even in the inner-shelf, the cross-shelf momentum balance is mostly controlled by a geostrophic equilibrium between the cross-shelf pressure gradient and Coriolis. Intensification of the along-shelf velocities (e.g., March-April) controls the size of the geostrophic equilibrium and thus the cross-shelf momentum balance. Only when the along-shelf flow is reduced (e.g., November), the frictional effects may increase their importance in the cross-shelf momentum balance.

[53] **Acknowledgments.** The authors would like to acknowledge Neil Ganju (USGS, Woods Hole), Thomas Connolly (WHOI, Woods Hole), and Steve Lentz (WHOI, Woods Hole) for their comments and suggestions. The manuscript was also improved due to the suggestions of two anonymous reviewers. The research leading to these results has received funding from the European Community's Seventh Framework Programme (FP7/2007/2013) under grant agreement 242284 (Field_ac project). The authors also want to acknowledge the MAR2 (Mar Y Medio Ambiente Marino, MARYAM 2013), COVARIANCE (CTM-2010-19709), and Neptune (Neptune/-EIT/KIC InnoEnergy) projects.

References

Allen, J. S., and P. K. Kundu (1978), On the momentum, vorticity and mass balance on the Oregon Shelf, *J. Phys. Oceanogr.*, *8*(1), 13–27.

Blayo, E., and L. Debreu (2005), Revisiting open boundary conditions from the point of view of characteristic variables, *Ocean Modell.*, *9*(3), 231–252.

Bolaños, R., G. Jorda, J. Cateura, J. Lopez, J. Puigdefabregas, J. Gomez, and M. Espino (2009), The XIOM: 20 years of a regional coastal observatory in the Spanish Catalan coast, *J. Mar. Syst.*, *77*(3), 237–260.

Bolaños-Sanchez, R., A. Sanchez-Arcilla, and J. Cateura (2007), Evaluation of two atmospheric models for wind–wave modelling in the NW Mediterranean, *J. Mar. Syst.*, *65*(1-4), 336–353.

Castellari, S., N. Pinardi, and K. Leaman (1998), A model study of air-sea interactions in the Mediterranean Sea, *J. Mar. Syst.*, *18*, 89–114.

Fewings, M., S. J. Lentz, and J. Fredericks (2008), Observations of cross-shelf flow driven by cross-shelf winds on the inner continental shelf, *J. Phys. Oceanogr.*, *38*(11), 2358–2378.

Fewings, M. R., and S. J. Lentz (2010), Momentum balances on the inner continental shelf at Martha's Vineyard Coastal Observatory, *J. Geophys. Res.*, *115*, C12023, doi:10.1029/2009JC005578.

Font, J. (1990), A comparison of seasonal winds with currents on the continental slope of the Catalan Sea (northwestern Mediterranean), *J. Geophys. Res.*, *95*(C2), 1537–1545.

Font, J., J. Salat, and J. Tintoré (1988), Permanent features of the circulation in the Catalan sea, in *Pelagic Mediterranean Oceanography*, edited by H. J. Minas and P. Nival, Oceanol. Acta, *9*(vol. sp.), 51–57.

Font, J., E. Garcia-Ladona, and E. G. Górriz (1995), The seasonality of mesoscale motion in the Northern Current of the Western Mediterranean several years of evidence, *Oceanol. Acta*, *18*(2), 207–219.

Grifoll, M., A. L. Aretxabaleta, M. Espino, and J. C. Warner (2012), Along-shelf current variability on the Catalan inner-shelf (NW Mediterranean), *J. Geophys. Res.*, *117*, C09027, doi:10.1029/2012JC008182.

Hickey, B. M. (1984), The fluctuating longshore pressure gradient on the Pacific Northwest Shelf: A dynamical analysis, *J. Phys. Oceanogr.*, *14*(2), 276–293.

Hickey, B. M., E. L. Dobbins, and S. E. Allen (2003), Local and remote forcing of currents and temperature in the central Southern California Bight, *J. Geophys. Res.*, *108*(C3), 3081, doi:10.1029/2000JC000313.

Holt, J. T., J. I. Allen, R. Proctor, and F. Gilbert (2005), Error quantification of a high-resolution coupled hydrodynamic-ecosystem coastal-ocean model. Part 1: Model overview and assessment of the hydrodynamics, *J. Mar. Syst.*, *57*, 167–188.

Jansá, A., A. Genoves, M. A. Picornell, J. Campins, D. Radinovic, and P. Alpert (1994), Mediterranean cyclones: Subject of a WMO project, in *The Life Cycle of Extratropical Cyclones*, vol. *2*, pp. 26–31, Bergen.

Jordi, A., A. Orfila, G. Basterretxea, and J. Tintoré (2005), Coastal trapped waves in the northwestern Mediterranean, *Cont. Shelf Res.*, *25*(2), 185–196.

Kantha, L. H., and C. A. Clayson (1994), An improved mixed layer model for geophysical applications, *J. Geophys. Res.*, *99*, 25,235–25,266.

Lee, T. N., E. Williams, R. E. J. Wang, and L. Atkinson (1989), Response of South Carolina continental shelf waters to wind and Gulf Stream forcing during winter of 1986, *J. Geophys. Res.*, *94*, 10,715–10,754.

Lentz, S. J. (1994), Current dynamics over the Northern California Inner Shelf, *J. Phys. Oceanogr.*, *24*(12), 2461–2478.

Lentz, S. J., and D. C. Chapman (2004), The importance of nonlinear cross-shelf momentum flux during wind-driven coastal upwelling, *J. Phys. Oceanogr.*, *34*, 2444–2457.

Lentz, S. J., and M. R. Fewings (2012), The wind- and wave-driven inner-shelf circulation, *Annu. Rev. Mar. Sci.*, *4*(1), 317–343.

Lentz, S. J., and C. D. Winant (1986), Subinertial currents on the Southern California Shelf, *J. Phys. Oceanogr.*, *16*(11), 1737–1750.

Lentz, S., R. T. Guza, S. Elgar, F. Feddersen, and T. H. C. Herbers (1999), Momentum balances on the North Carolina inner shelf, *J. Geophys. Res.*, *104*(C8), 18,205–18,226.

Lionello, P., J. Bhend, A. Buzzi, P. M. Della-Marta, S. Krichak, A. Jansà, P. Maheras, A. Sanna, I. F. Trigo, and R. Trigo (2006), Cyclones in the Mediterranean region: Climatology and effects on the environment, in *Mediterranean Climate Variability*, edited by P. Lionello, P. Malanotte-Rizzoli, and R. Boscolo, pp. 324–372, Elsevier, Amsterdam.

Liquete, C., M. Canals, W. Ludwig, and P. Arnau (2009), Sediment discharge of the rivers of Catalonia, NE Spain, and the influence of human impacts, *J. Hydrol.*, *366*(1–4), 76–88.

Liu, Y., and R. H. Weisberg (2005), Momentum balance diagnoses for the West Florida Shelf, *Cont. Shelf Res.*, *25*(17), 2054–2074.

Marcos, M., and M. N. Tsimplis (2007), Variations of the seasonal sea level cycle in southern Europe, *J. Geophys. Res.*, *112*, C12011, doi:10.1029/2006JC004049.

Mason, E., and A. Pascual (2012), Multiscale variability in the Balearic Sea: An altimetric perspective, *J. Geophys. Res. Oceans*, *118*, 3007–3025, doi:10.1002/jgrc.20234.

Mason, E., J. Molemaker, A. F. Shchepetkin, F. Colas, J. C. McWilliams, and P. Sangrà (2010), Procedures for offline grid nesting in regional ocean models, *Ocean Modell.*, *35*(1-2), 1–15.

Maza, M., G. Voulgaris, and B. Subrahmanyam (2006), Subtidal inner shelf currents off Cartagena de Indias, Caribbean coast of Colombia, *Geophys. Res. Lett.*, *33*(21), 1–5.

Millot, C. (1999), Circulation in the western Mediterranean Sea, *J. Mar. Syst.*, *20*(1–4), 423–442.

O'Neill, C. K., J. A. Polton, J. T. Holt, and E. J. O'Dea (2012) Modelling temperature and salinity in Liverpool Bay and the Irish Sea: Sensitivity to model type and surface forcing, *Ocean Sci.*, *8*, 903–913.

Petrenko, A. A (2003), Variability of circulation features in the Gulf of Lion NW Mediterranean Sea. Importance of inertial currents, *Oceanol. Acta*, *26*(4), 323–338, doi:10.1016/S0399-1784(03)00038-0.

Renault, L., J. Chiggiato, J. C. Warner, M. Gomez, G. Vizoso, and J. Tintoré (2012), Coupled atmosphere-ocean-wave simulations of a storm event over the Gulf of Lion and Balearic Sea, *J. Geophys. Res. 117*, C09019, doi:10.1029/2012JC007924.

Rodi, W. (1987), Examples of calculation methods for flow and mixing in stratified fluids, *J. Geophys. Res.*, *92*(C5), 5305–5328.

Salat, J., J. Tintore, J. Font, D.-P. Wang, and M. Vieira (1992), Near-inertial motion on the shelf-slope front off Northeast Spain, *J. Geophys. Res.*, *97*(C5), 7277–7281.

Salat, J., M. A. Garcia, A. Cruzado, A. Palanques, L. Arín, D. Gomis, J. Guillén, A. de León, J. Puigdefàbregas, J. Sospedra, Z. R. Velásquez (2002), Seasonal changes mass structure and shelf slope at the Ebre Shelf (NW Mediterranean), *Cont. Shelf Res.*, *22*, 327–348.

Sánchez-Arcilla, A., and J. H. Simpson (2002), The narrow shelf concept: Couplings and fluxes, *Cont. Shelf Res.*, *22*(2), 153–172.

Schaeffer, A., P. Garreau, A. Molcard, P. Fraunié, and Y. Seity (2011), Influence of high-resolution wind forcing on hydrodynamic modeling of the Gulf of Lions, *Ocean Dyn.*, *61*, 1823–2844.

Shchepetkin, A. F., and J. C. McWilliams (2005), The regional oceanic modeling system (ROMS): A split-explicit, free-surface, topography-following-coordinate oceanic model, *Ocean Modell.*, *9*(4), 347–404.

Taylor, K. E. (2001), Summarizing multiple aspects of model performance in a single diagram, *J. Geophys. Res.*, *106*, 7183–7192.

Tilburg, C. E. (2003), Across-shelf transport on a continental shelf: Do across-shelf winds matter?, *J. Phys. Oceanogr. 33*, 2675–2688.

Tonani, M., N. Pinardi, C. Fratianni, J. Pistoia, S. Dobricic, S. Pensieri, M. de Alfonso, and K. Nittis (2009), Mediterranean forecasting system: Forecast and analysis assessment through skill scores, *Ocean Sci.*, *5*(4), 649–660.

Umlauf, L., and H. Burchard (2003), A generic length-scale equation for geophysical turbulence models, *J. Mar. Res.*, *61*, 235–265.

Warner, J. C., C. R. Sherwood, H. G. Arango, and R. P. Signell (2005), Performance of four turbulence closure models implemented using a generic length scale method, *Ocean Modell.*, *8*(1-2), 81–113.

Winant, C. D., R. C. Beardsley, and R. E. Davis (1987), Moored wind, temperature and current observations made during coastal ocean dynamics experiments 1 and 2 over the Northern California continental shelf and upper slope, *J. Geophys. Res.*, *92*(C2), 1569–1604.